Search for gamma rays from dark matter annihilations around intermediate mass black holes with the HESS experiment

F. Aharonian,[1,14] A. G. Akhperjanian,[2] U. Barres de Almeida,[8,*] A. R. Bazer-Bachi,[3] B. Behera,[14] M. Beilicke,[4] W. Benbow,[1] K. Bernlöhr,[1,5] G. Bertone,[6,+] C. Boisson,[7] A. Bochow,[1] V. Borrel,[3] I. Braun,[1] E. Brion,[8] J. Brucker,[17] P. Brun,[8] R. Bühler,[1] T. Bulik,[25] I. Büsching,[10] T. Boutelier,[18] S. Carrigan,[1] P. M. Chadwick,[9] R. C. G. Chaves,[1] L.-M. Chounet,[11] A. C. Clapson,[1] G. Coignet,[12] L. Costamante,[1,30] M. Dalton,[5] B. Degrange,[11] H. J. Dickinson,[9] A. Djannati-Ataï,[13] W. Domainko,[1] L. O'C. Drury,[14] F. Dubois,[12] G. Dubus,[18] J. Dyks,[25] K. Egberts,[1] D. Emmanoulopoulos,[15] P. Espigat,[13] C. Farnier,[16] F. Feinstein,[16] A. Fiasson,[16] A. Förster,[1] G. Fontaine,[11] M. Füßling,[5] S. Gabici,[14] Y. A. Gallant,[16] L. Gérard,[13] B. Giebels,[11] J. F. Glicenstein,[8] B. Glück,[17] P. Goret,[8] C. Hadjichristidis,[9] D. Hauser,[15] M. Hauser,[15] G. Heinzelmann,[4] G. Henri,[18] G. Hermann,[1] J. A. Hinton,[26] A. Hoffmann,[19] W. Hofmann,[1] M. Holleran,[10] S. Hoppe,[1] D. Horns,[4] A. Jacholkowska,[16] O. C. de Jager,[10] I. Jung,[17] K. Katarzyński,[28] S. Kaufmann,[15] E. Kendziorra,[19] M. Kerschhaggl,[5] D. Khangulyan,[1] B. Khélifi,[11] D. Keogh,[9] Nu. Komin,[16] K. Kosack,[1] G. Lamanna,[12] I. J. Latham,[9] J.-P. Lenain,[7] T. Lohse,[5] V. Marandon,[13] J. M. Martin,[7] O. Martineau-Huynh,[20] A. Marcowith,[16] C. Masterson,[14] D. Maurin,[20] T. J. L. McComb,[9] R. Moderski,[25] E. Moulin,[8,‡] M. Naumann-Godo,[11] M. de Naurois,[20] D. Nedbal,[21] D. Nekrassov,[1] J. Niemiec,[29] S. J. Nolan,[9] S. Ohm,[1] J-P. Olive,[3] E. de OñaWilhelmi,[13,30] K. J. Orford,[9] J. L. Osborne,[9] M. Ostrowski,[24] M. Panter,[1] G. Pedaletti,[15] G. Pelletier,[18] P.-O. Petrucci,[18] S. Pita,[13] G. Pühlhofer,[15] M. Punch,[13] A. Quirrenbach,[15] B. C. Raubenheimer,[10] M. Raue,[1,30] S. M. Rayner,[9] M. Renaud,[1] F. Rieger,[1,30] J. Ripken,[4] L. Rob,[21] S. Rosier-Lees,[12] G. Rowell,[27] B. Rudak,[25] J. Ruppel,[22] V. Sahakian,[2] A. Santangelo,[19] R. Schlickeiser,[22] F. M. Schöck,[17] R. Schröder,[22] U. Schwanke,[5] S. Schwarzburg,[19] S. Schwemmer,[15] A. Shalchi,[22] J. L. Skilton,[26] H. Sol,[7] D. Spangler,[9] Ł. Stawarz,[24] R. Steenkamp,[23] C. Stegmann,[17] G. Superina,[11] P. H. Tam,[15] J.-P. Tavernet,[20] R. Terrier,[13] O. Tibolla,[15] C. van Eldik,[1] G. Vasileiadis,[16] C. Venter,[10] J. P. Vialle,[12] P. Vincent,[20] M. Vivier,[8] H. J. Völk,[1] F. Volpe,[11,30] S. J. Wagner,[15] M. Ward,[9] A. A. Zdziarski,[25] and A. Zech[7]

[1]*Max-Planck-Institut für Kernphysik, P.O. Box 103980, D 69029 Heidelberg, Germany*
[2]*Yerevan Physics Institute, 2 Alikhanian Brothers Street, 375036 Yerevan, Armenia*
[3]*Centre d'Etude Spatiale des Rayonnements, CNRS/UPS, 9 av. du Colonel Roche, BP 4346, F-31029 Toulouse Cedex 4, France*
[4]*Universität Hamburg, Institut für Experimentalphysik, Luruper Chaussee 149, D 22761 Hamburg, Germany*
[5]*Institut für Physik, Humboldt-Universität zu Berlin, Newtonstr. 15, D 12489 Berlin, Germany*
[6]*Institut d'Astrophysique de Paris, UMR 7095 CNRS, Université Pierre et Marie Curie, 98 bis boulevard Arago, 75014 Paris, France*
[7]*LUTH, Observatoire de Paris, CNRS, Université Paris Diderot, 5 Place Jules Janssen, 92190 Meudon, France*
[8]*IRFU/DSM/CEA, CE Saclay, F-91191 Gif-sur-Yvette, Cedex, France*
[9]*University of Durham, Department of Physics, South Road, Durham DH1 3LE, U.K.*
[10]*Unit for Space Physics, North-West University, Potchefstroom 2520, South Africa*
[11]*Laboratoire Leprince-Ringuet, Ecole Polytechnique, CNRS/IN2P3, F-91128 Palaiseau, France*
[12]*Laboratoire d'Annecy-le-Vieux de Physique des Particules, CNRS/IN2P3, 9 Chemin de Bellevue - BP 110 F-74941 Annecy-le-Vieux Cedex, France*
[13]*Astroparticule et Cosmologie (APC), CNRS, Université Paris 7 Denis Diderot, 10, rue Alice Domon et Leonie Duquet, F-75205 Paris Cedex 13, France*[§]
[14]*Dublin Institute for Advanced Studies, 5 Merrion Square, Dublin 2, Ireland*
[15]*Landessternwarte, Universität Heidelberg, Königstuhl, D 69117 Heidelberg, Germany*
[16]*Laboratoire de Physique Théorique et Astroparticules, CNRS/IN2P3, Université Montpellier II, CC 70, Place Eugène Bataillon, F-34095 Montpellier Cedex 5, France*
[17]*Universität Erlangen-Nürnberg, Physikalisches Institut, Erwin-Rommel-Str. 1, D 91058 Erlangen, Germany*
[18]*Laboratoire d'Astrophysique de Grenoble, INSU/CNRS, Université Joseph Fourier, BP 53, F-38041 Grenoble Cedex 9, France*
[19]*Institut für Astronomie und Astrophysik, Universität Tübingen, Sand 1, D 72076 Tübingen, Germany*
[20]*LPNHE, Université Pierre et Marie Curie Paris 6, Université Denis Diderot Paris 7, CNRS/IN2P3, 4 Place Jussieu, F-75252, Paris Cedex 5, France*
[21]*Institute of Particle and Nuclear Physics, Charles University, V Holesovickach 2, 180 00 Prague 8, Czech Republic*
[22]*Institut für Theoretische Physik, Lehrstuhl IV: Weltraum und Astrophysik, Ruhr-Universität Bochum, D 44780 Bochum, Germany*
[23]*University of Namibia, Private Bag 13301, Windhoek, Namibia*
[24]*Obserwatorium Astronomiczne, Uniwersytet Jagielloński, ul. Orla 171, 30-244 Kraków, Poland*
[25]*Nicolaus Copernicus Astronomical Center, ul. Bartycka 18, 00-716 Warsaw, Poland*
[26]*School of Physics & Astronomy, University of Leeds, Leeds LS2 9JT, UK*
[27]*School of Chemistry & Physics, University of Adelaide, Adelaide 5005, Australia*
[28]*Toruń Centre for Astronomy, Nicolaus Copernicus University, ul. Gagarina 11, 87-100 Toruń, Poland*

[29]*Instytut Fizyki Jądrowej PAN, ul. Radzikowskiego 152, 31-342 Kraków, Poland*
[30]*European Associated Laboratory for Gamma-Ray Astronomy, jointly supported by CNRS and MPG*
(Received 22 April 2008; published 30 October 2008)

The HESS array of Cherenkov telescopes has performed, from 2004 to 2007, a survey of the inner galactic plane at photon energies above 100 GeV. About 400 hours of data have been accumulated in the region between −30 and +60 degrees in galactic longitude, and between −3 and +3 degrees in galactic latitude. Assuming that dark matter is composed of weakly interacting massive particles, we calculate here the HESS sensitivity map for dark matter annihilations, and derive the first experimental constraints on the (''minispikes'') scenario, in which a gamma-ray signal arises from dark matter annihilation around intermediate mass black holes. The data exclude the proposed scenario at a 90% confidence level for dark matter particles with velocity-weighted annihilation cross section σv above 10^{-28} cm^3 s^{-1} and mass between 800 GeV and 10 TeV.

DOI: 10.1103/PhysRevD.78.072008 PACS numbers: 98.70.Rz, 95.35.+d, 98.56.Wm

I. INTRODUCTION

A substantial body of cosmological and astrophysical measurements suggests that ~22% of the Universe is composed of nonbaryonic dark matter (DM), e.g. [1], commonly assumed to be in the form of weakly interacting massive particles (WIMPs) arising in extensions of the standard model of particle physics (for recent reviews see [2,3]). The lightest neutralino arising in supersymmetric (SUSY) extensions of the standard model [4], and the first excitation of the Kaluza-Klein bosons $\tilde{B}^{(1)}$ in universal extra dimension (UED) theories [5–7] are among the most widely discussed dark matter candidates.

Although accelerator and direct dark matter searches may well provide useful hints on the nature of dark matter, a correct identification is likely to require the combination of different techniques, including the indirect searches, based on the detection of the annihilation products of dark matter particles. The annihilation rate being proportional to the square of the dark matter density integrated along the line of sight, regions with enhanced dark matter density are primary targets of indirect searches. Among them are the galactic halo [8], external galaxies [9], galaxy clusters [10], substructures [11–19], and the Galactic Center (GC) [20–24].

The GC, in particular, has attracted significant interest. The distribution of dark matter at the GC is actually highly uncertain, due to lack of resolution in N-body simulations, and to the many astrophysical effects that further complicate the situation, such as the presence of the supermassive black hole coincident with Sgr A*, gravitational scattering of dark matter off the stellar cusp, and dark matter annihilation [25].

Dwarf spheroidal galaxies in the Local Group[26] have also been considered as targets for gamma-ray detection, since they seem to represent dark matter dominated regions [27–32]. More recently, the Sloan Digital Sky Survey revealed the existence of new satellites [33–35] offering appealing features for dark matter searches. Radial velocity dispersion of stars in galaxy satellites usually implies large mass-to-luminosity ratio. Nevertheless, the lack of accurate measurements on the velocity dispersion may induce large systematic effects on the parameters used for the modelling of the dark matter halo. Even in the case of accurate kinematic data for some of the galaxy satellites, only faint annihilation signals are expected for smooth dark matter halos due to their distance of ~100 kpc.

Minispikes around intermediate mass black holes (IMBHs) have been recently proposed as promising targets for indirect dark matter detection [36]. Accurate predictions, in the context of well-defined astrophysical scenarios, have been derived for the distribution and luminosity of these objects [37]. Minispikes might in fact be detected as bright pointlike sources in gamma rays [38] and neutrinos [39], and the prospects for detection with satellites with large field of view such as the upcoming GLAST experiment [40] to be launched in 2008 appear particularly promising.

Current imaging atmospheric Cherenkov telescopes can also effectively search for these objects. The HESS (High Energy Stereoscopic System) experiment has already surveyed a significant part of the galactic plane. With the combination of a large field of view, very good angular resolution and off-axis performance, HESS has reached the sensitivity to accurately map the galactic plane in scan-based observations.

In this paper, HESS data are used to derive for the first time experimental exclusion limits on the dark matter annihilation signals within the context of the minispike scenario. The paper is organized as follows. Sec. II is devoted to the minispike scenario and the gamma-ray

*Supported by CAPES Foundation, Ministry of Education of Brazil.
+Not a HESS member; bertone@iap.fr
‡emmanuel.moulin@cea.fr
§Also at UMR 7164 (CNRS, Université Paris VII, CEA, Observatoire de Paris).

flux expected from dark matter annihilations in minispikes. In Sec. III, we present the HESS data from the galactic plane survey and compute the HESS flux sensitivity map to dark matter annihilations in the galactic plane region. Exclusion limits are then derived for dark matter annihilation from minispikes. Finally, Sec. IV is devoted to the discussion of the results obtained in this study.

II. DARK MATTER ANNIHILATIONS IN MINISPIKES

A. Dark matter candidates in MSSM and Kaluza-Klein models

In this paper, we focus on two particle physics scenarios beyond the standard model, which provide well-motivated WIMP dark matter candidates with masses and couplings at the electroweak scale to account for the nonbaryonic dark matter. The annihilation of WIMP pairs can produce in the final state a continuum of gamma-rays whose flux extends up to the DM particle mass, from the hadronization and decay of the cascading annihilation products.

Minimal supersymmetric extensions of the standard model (MSSM) predict the lightest supersymmetric particle (LSP) to be stable in the case of R-parity conserving scenarios [4]. In various SUSY breaking schemes, this fermionic particle is the lightest neutralino χ. In general MSSM, the gamma-ray spectrum from neutralino annihilation is not uniquely determined and the branching ratios (BRs) of the open annihilation channels are not determined, since the DM particle field content is not known. Soft and hard spectra for the neutralino pair annihilation are therefore considered. The annihilation spectra are parametrized using PYTHIA [41] simulations. Figure 1 shows the number of gammas above the energy threshold $E_{\rm th} = 100$ GeV, $N_\gamma(E_\gamma > E_{\rm th})$, as a function of the neutralino mass m_χ. $N_\gamma(E_\gamma > E_{\rm th})$ is lower in the case of a 100% BR $b\bar{b}$ channel than in the $\tau^+\tau^-$ channel for m_χ below 2 TeV. Above 2 TeV, more gammas are expected in the $b\bar{b}$ channel.

In some specific scenarios, the branching ratios of the annihilation channels can be computed given that the field content of the DM particle is known. In the SUSY scenario dubbed AMSB [42–45] (anomaly mediated supersymmetry breaking) arising in SUSY theories [46,47], the DM candidate is the lightest neutralino with a predominant wino component, which annihilates in W^+W^- pairs decaying in quarks and leptons. Large annihilation cross sections are expected, which may lead to detectable gamma-ray fluxes [48]. Within this scenario, neutralino masses may extend up to tens of TeV. The other dark matter candidate considered here arises in theories with UED. In Kaluza-Klein (KK) scenarios with KK-parity conservation, the lightest KK particle (LKP) is stable. Most often, the LKP is the first KK mode of the hypercharge gauge boson, referred hereafter to as $\tilde{B}^{(1)}$ [5–7]. In the Kaluza-Klein case, the BRs are extracted from [7]. $\tilde{B}^{(1)}$ pairs annihilate mainly into fermion pairs: 35% in quark pairs and 59% in charged lepton pairs.

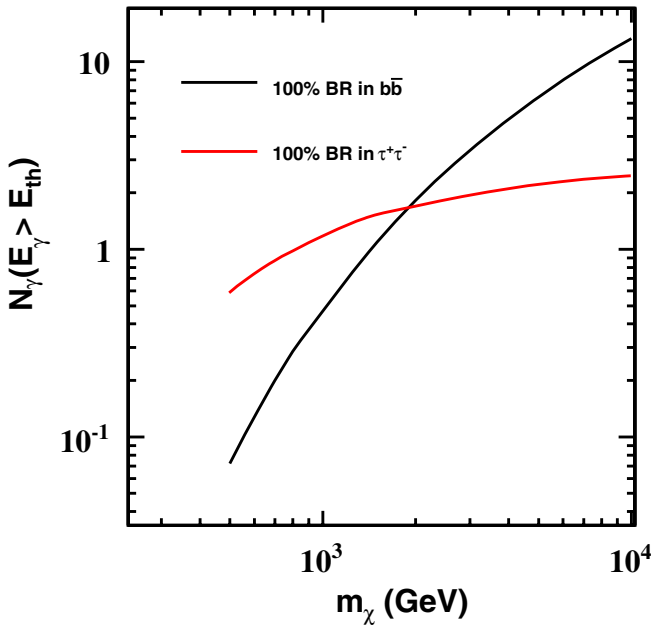

FIG. 1 (color online). Number of gammas per annihilation above the energy threshold $E_{\rm th} = 100$ GeV, $N_\gamma(E_\gamma > E_{\rm th})$, as a function of the neutralino mass, m_χ, for 100% BR in the $b\bar{b}$ channel (solid black line) and 100% BR in the $\tau^+\tau^-$ (solid red line). This number corresponds to the annihilation spectrum integrated from $E_{\rm th}$ up to m_χ. Below 2 TeV neutralino masses, more gammas per annihilation are expected in the case of the $\tau^+\tau^-$ channel than for $b\bar{b}$, thus the latter will provide a conservative value. Above 2 TeV, the $b\bar{b}$ channel yields more gammas than the $\tau^+\tau^-$ one.

B. IMBHs formation scenarios

IMBHs are compact objects with masses comprised between that of the heaviest remnant of a stellar collapse, $\sim 20 M_\odot$ [49,50], and the lower end of the mass range of supermassive black holes (SMBH) $\sim 10^6 M_\odot$ [51,52].

Observational hints of the existence of IMBHs come from the detection of ultraluminous x-ray sources , apparently not associated with active galactic nuclei [53–55], from stellar kinematics in globular clusters [56,57] and emission-line time lags in galaxies [58].

From a theoretical point of view, a population of massive seed black holes could help to explain the origin of SMBHs, especially those powering quasars at redshift 6 or 7, that were thus already in place when the Universe was only ~ 1 Gyr old [59]. A population of IMBHs is in fact a generic prediction of scenarios that seek to explain the properties of supermassive black holes [60–62]. However, despite their theoretical interest, it is difficult to obtain conclusive evidence for the existence of IMBHs.

In Ref. [38], the consequences of the formation and growth of IMBHs on the surrounding distribution of DM have been studied. In particular, it was shown that these processes lead to the formation of strong dark matter overdensities called *minispikes*, which are ideal targets for indirect dark matter searches, as they would appear as a population of gamma-ray point-sources with identical energy spectrum.

The properties of minispikes have been discussed in detail for two different scenarios. In the first one (scenario A), black holes are remnants of the collapse of Population III (or ''first'') stars [63], which are believed to collapse directly to black holes in the mass range $M \sim 60$–$140 M_\odot$ and $M \gtrsim 260 M_\odot$ [64]. Black holes in this scenario may not necessarily form at the very centers of their initial host dark matter halos at high redshift, a circumstance that, as we shall see, may have important consequences on the detectability of IMBHs.

The second scenario (scenario B) is representative of a class of models in which black holes originate from the collapse of primordial gas in early-forming halos [62,65–70]. The initial black holes are massive ($\sim 10^5 M_\odot$) and the growth of SMBH proceeds in such a way that both mergers and accretion play an important role. Following Ref. [38], we focus here on the specific formation scenario proposed in Ref. [62], which goes as follows: during the virialization and collapse of the first halos, gas cools, collapses, and forms pressure-supported disks at the centers of halos that are sufficiently massive to contain a relatively large amount of molecular hydrogen. Local gravitational instabilities in the disk lead to an effective viscosity that transfers mass inward and angular momentum outward [71] until supernovæ in the first generation of stars heat the disk and terminate this process [62]. By the time the process terminates (of the order of the lifetimes of Population III stars, ~1–10 Myr), a baryonic mass of order $\sim 10^5 M_\odot$ has lost its angular momentum and has been transferred to the center of the halo. Such an object may be briefly pressure supported, but it eventually collapses to form a black hole [64,72].

The characteristic mass of the black hole forming in a halo of virial mass M_v is given by [62]

$$M_{\rm bh} = 3.8 \times 10^4 M_\odot \left(\frac{\kappa}{0.5}\right)\left(\frac{f}{0.03}\right)^{3/2}\left(\frac{M_v}{10^7 M_\odot}\right)\left(\frac{1+z}{18}\right)^{3/2} \times \left(\frac{t}{10\ {\rm Myr}}\right), \quad (1)$$

where f is the fraction of the total baryonic mass in the halo that falls into the disk, z is the redshift of formation, κ is the fraction of the baryonic mass that loses its angular momentum and remains in the remnant black hole, and t is the timescale for the evolution of the first generation of stars [62].

In order to study the consequences for indirect dark matter searches we will compare HESS data with the mock catalogs of Ref. [38], which consisted of 200 stochastic realizations of Milky Way-like halos at $z = 0$, obtained by populating halos with black holes at high redshift (following the prescriptions of scenarios A and B) and evolving them forward to determine the properties of satellite black holes. The mass of the Milky Way was fixed at $10^{12.1} h^{-1} M_\odot$ at $z = 0$, and our analysis is based on their statistically large sample of wandering black hole populations in Milky Way-like halos of this mass.

In scenario A, the mass spectrum of unmerged black holes is a delta function and the average number of *unmerged* black holes per Milky Way halo is $N_{\rm bh,A} \simeq 1027 \pm 84$, where the error bar denotes the 1σ scatter from halo to halo [73]. In scenario B, the total number of *unmerged* black holes per Milky Way halo is $N_{\rm bh,B} \simeq 101 \pm 22$ [38]. The dispersion denotes the 1σ scatter among different realizations of Milky Way-like halos, as discussed in [38].

C. Minispikes

The growth of massive black holes inevitably affects the surrounding distribution of dark matter. The profile of the final DM overdensity, called *minispike*, depends on the initial distribution of matter, but also on astrophysical processes such as gravitational scattering off stars and mergers.

Ignoring astrophysical effects, and assuming adiabatic growth of the black hole (i.e. assuming that the black hole grows on a time scale much longer than the dynamical time scales of DM around it), one can calculate analytically the functional form of the final DM profile. If one starts from an initially uniform DM distribution, which is the most likely situation for black holes in scenario A, the final profile will be a mild minispike with density $\rho_{\rm sp} \propto (r/r_h)^{3/2}$ (e.g. see [74] and references therein). If one starts from a cuspy profile that is a power law with index $\gamma = 1$, as relevant for scenario B, the new profile is a new power law,

$$\rho_{\rm sp}(r) = \rho(r_{\rm sp})\left(\frac{r}{r_{\rm sp}}\right)^{-\gamma_{\rm sp}} \quad (2)$$

where the radius of the spike is $r_{\rm sp} \approx 0.2 r_h$ [75], and $\gamma_{\rm sp}$ is related to the initial power-law index γ by [76]

$$\gamma_{\rm sp} = \frac{9 - 2\gamma}{4 - \gamma}. \quad (3)$$

In the case of the Navarro, Frenk, and White (NFW) profile, $\gamma = 1$, which implies $\gamma_{\rm sp} = 7/3$.

To calculate the annihilation flux, the singularity of $\rho_{\rm sp}$ at $r = 0$ needs to be cut off; we introduce a minimal radius $r_{\rm cut}$. One limit is given by the size of the IMBH, another by the condition that the annihilation rate of the dark matter

particles is smaller than the inverse age of the minispike

$$\rho_{\rm sp}(r_{\rm lim}) = m_\chi/\sigma v(t - t_f) \equiv \rho_{\rm lim}. \quad (4)$$

An inner cutoff is therefore defined at a radius

$$r_{\rm cut} = \max[4R_{\rm Schw}, r_{\rm lim}], \quad (5)$$

where $R_{\rm Schw}$ is the Schwarzschild radius of the IMBH $R_{\rm Schw} = 2.95\ {\rm km}\, M_{\rm bh}/M_\odot$. For common values of the mass and cross section of the DM particle, $r_{\rm lim} \sim 10^{-3}$ pc so that $r_{\rm cut} = r_{\rm lim}$.

Although in principle this applies also to the black hole at the Galactic Center, there are a number of astrophysical effects, such as off-center formation, major mergers, and gravitational scattering off stars, that tend to erase any DM overdensity. A detailed discussion of the formation and evolution of the DM spike at the Galactic Center, including a discussion of the prospects for indirect detection in light of the very high energy (VHE, $E_\gamma > 100$ GeV) gamma-ray source coincident with Sgr A*, can be found in Ref. [25].

All these astrophysical processes are unlikely to take place around IMBHs. Minispikes around IMBHs that *never experience mergers* are therefore expected to be stable structures over cosmological timescales, and they are thus promising targets for indirect detection. The gamma-ray flux from these targets can be easily calculated, once the DM profile has been determined with the prescription outlined above. In the case of scenario B, which leads to higher gamma-ray fluxes than scenario A, the differential flux from a minispike at distance D can be written as [38]

$$\Phi(E, D) = \Phi_0 \frac{{\rm d}N}{{\rm d}E}\left(\frac{\sigma v}{10^{-26}\ {\rm cm^3\ s^{-1}}}\right)\left(\frac{m_\chi}{100\ {\rm GeV}}\right)^{-2} \times \left(\frac{D}{\rm kpc}\right)^{-2}\left(\frac{\rho(r_{\rm sp})}{10^2\ {\rm GeV\,cm^{-3}}}\right)^2\left(\frac{r_{\rm sp}}{\rm pc}\right)^{14/3} \times \left(\frac{r_{\rm cut}}{10^{-3}\ {\rm pc}}\right)^{-(5/3)}, \quad (6)$$

with $\Phi_0 = 9 \times 10^{-10}\ {\rm cm^{-2}\ s^{-1}}$. The gamma-ray spectrum per annihilation ${\rm d}N/{\rm d}E$ depends on the nature of the DM particle, and both numerical calculations and analytic fits are available in the literature for all possible annihilation channels. This formula is valid for minispikes forming adiabatically from an initial NFW profile, and under the (very good) approximation $r_{\rm sp} \gg r_{\rm cut}$. In this case, one can easily verify that the "luminosity" of a minispike in terms of DM annihilation is of the same order of magnitude as that of the entire Milky Way halo.

Although one would naively expect that the fluxes scale with $\sigma v/m_\chi^2$, in the minispike scenario the DM profile itself depends on m_χ and σv, and the final luminosity of

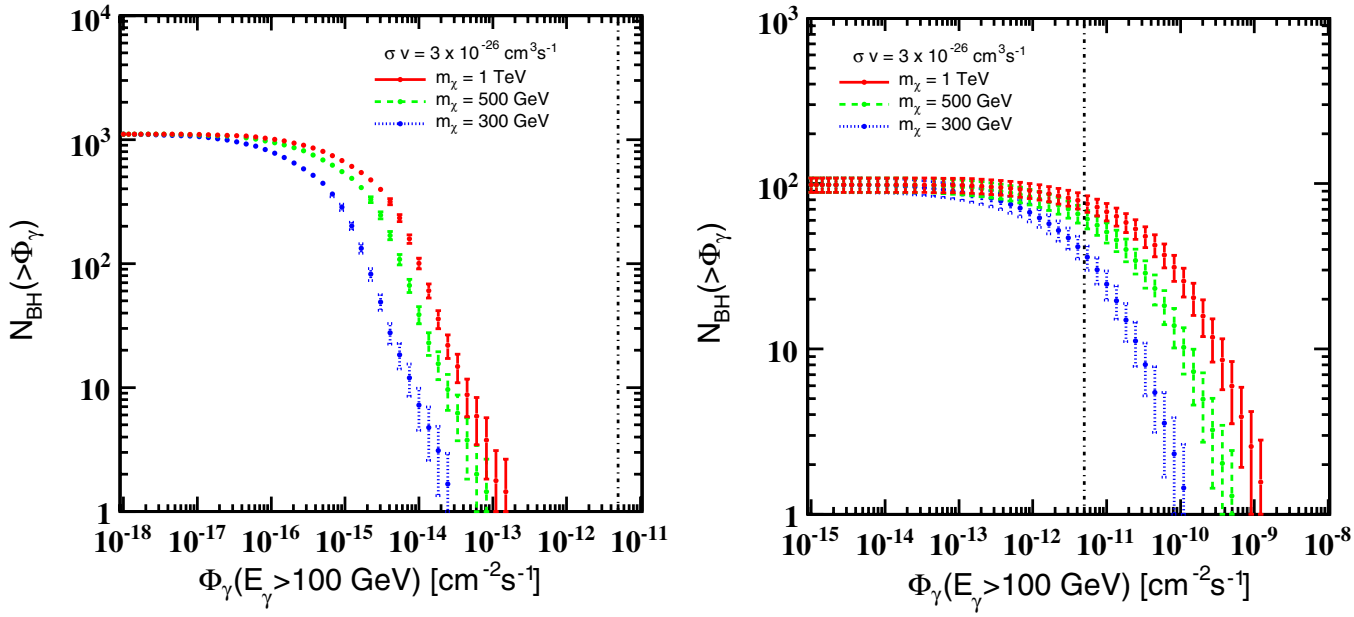

FIG. 2 (color online). Integrated luminosity function of IMBHs for the scenario A, i.e. for IMBH masses of $\sim 10^2\ {\rm M}_\odot$ (left), and the scenario B, i.e. for IMBH masses of $\sim 10^5\ {\rm M}_\odot$ (right), for a Milky Way-sized halo obtained from an average of 200 stochastic realizations (see text for details). Neutralino masses of 300, 500 GeV and 1 TeV, respectively, and a velocity-weighted annihilation cross section $\sigma v = 3 \times 10^{-26}\ {\rm cm^3\ s^{-1}}$ are considered. The integrated luminosity corresponds to the number of black holes yielding an integrated gamma-ray flux higher than a given integrated flux, $N_{\rm BH}(>\Phi_\gamma)$, as a function of the integrated flux Φ_γ. The gamma-ray flux is integrated above 100 GeV. The nominal 5σ HESS point source sensitivity (25 hours) is plotted (black dashed-dotted line) for comparison.

the objects, for an initially NFW profile, is proportional to $(\sigma v)^{2/7} m_\chi^{-9/7}$ [38].

Figure 2 shows the integrated luminosity function of IMBHs in a Milky Way-sized halo, i.e. the number of black holes $N_{\rm BH}$ producing an integrated gamma-ray flux higher than a given flux, as a function of the integrated flux. This can be understood as the number of black holes that can be detected with a telescope of given integrated flux sensitivity. The point-source sensitivity (5σ, 25 hours at 20° zenith) for HESS is plotted for comparison. The integrated luminosity is shown in the case of the aforementioned scenarios A and B, for three different dark matter particle masses and an annihilation cross section $\sigma v = 3 \times 10^{-26}$ cm^3 s^{-1}. This value allows for the thermal relic density of the DM particle to account for the measured cold dark matter density $\Omega_{\rm CDM} h^2 \simeq 0.1$ [see Eq. (3.4) of Ref. [4]]. Here, DM particles are assumed to be neutralinos annihilating in the $b\bar{b}$ channel. For the assumed value of σv, a large number of IMBHs in the Milky Way is within the reach of HESS for scenario B. In what follows, we will concentrate on that scenario. Figure 3 presents the mean integrated gamma-ray flux per IMBH for various energy thresholds as a function of the mass of the DM particle annihilating into $b\bar{b}$. Also displayed are the error bars corresponding to the root mean square (r.m.s) variation of the integrated flux distribution. For a 1 GeV threshold, well suited for gamma-ray satellite experiments, the maximum flux is obtained for a DM particle mass of ~80 GeV. This maximum comes from a balance between the factor $m_\chi^{-9/7}$ and the integral of the annihilation spectrum up to the DM particle mass [see Eq. (6)]. Adopting an energy threshold of 100 GeV, as appropriate for Cherenkov telescopes such as HESS, the largest fluxes are obtained for a mass of ~5 TeV. For this mass, the mean of the integrated flux distribution is 4.5×10^{-11} cm^{-2} s^{-1}. For masses close to the experimental threshold, the integrated flux increases with the dark matter mass. Well above the threshold, the standard regime is recovered, with fluxes decreasing with m_χ.

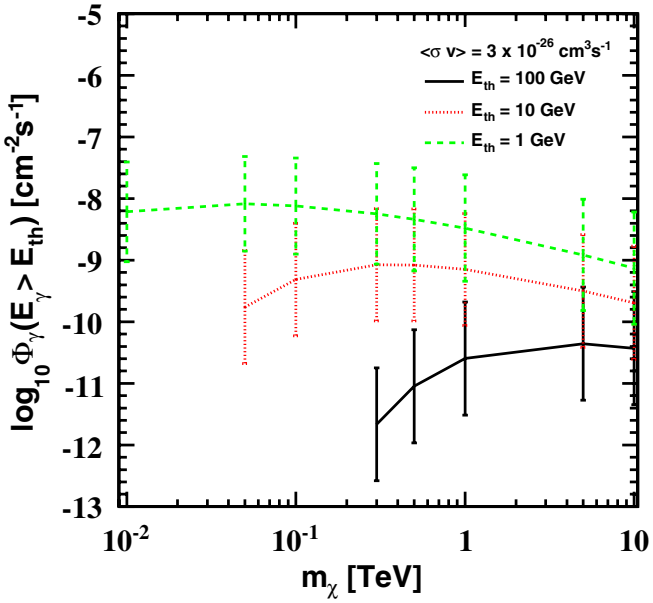

FIG. 3 (color online). Integrated flux Φ_γ expressed in cm^{-2} s^{-1} above the energy threshold as a function of the neutralino mass m_χ for thresholds of 1, 10, and 100 GeV, respectively, and a velocity-weighted annihilation cross section $\sigma v = 3 \times 10^{-26}$ cm^3 s^{-1}. The quoted error bars correspond to the r.m.s. of the integrated flux distribution. The maximum flux is obtained for neutralino masses well above the energy threshold of the instrument (see text for details).

III. HESS

A. The HESS instrument

The HESS array is dedicated to VHE gamma-ray astronomy. The instrument is composed of four imaging atmospheric Cherenkov telescopes located in the Khomas Highland of Namibia at an altitude of 1800 m above sea level. This southern location is well suited for observations toward the inner region of the galactic halo. Each telescope consists of an optical reflector of 107 m^2 composed of 382 round mirrors [77]. The Cherenkov light emitted by charged particles in the electromagnetic shower initiated by the primary gamma ray is focused onto a camera equipped with 960 photomultiplier tubes of 0.16° individual field of view [78]. The total field of view of HESS is 5° in diameter. The stereoscopic technique allows for accurate reconstruction of the direction and the energy of the primary gamma ray [79]. HESS has an angular resolution of about 5 arc minutes and a source location accuracy of ~30″ for strong sources. The sensitivity for pointlike sources reaches 2×10^{-13} cm^{-2} s^{-1} above 1 TeV for a 5σ detection in 25 hours at 20° zenith [80].

B. Observations and data analysis

The data used in this analysis were collected between 2004 and 2007 during the galactic plane survey with the four telescope HESS array. The galactic plane has been observed between ±3° in latitude and from −30° to 60° in longitude relative to the Galactic Center in 884 pointings. Runs are taken mainly with 28 min duration at pointing positions with a typical spacing of 0.4° in longitude and 1° in latitude. For the analysis described in this paper, the observations dedicated to known sources at other wavelengths are excluded. Astrophysical models of TeV emission are available for these sources so that the search is focused on regions where no standard astrophysical emitters have been detected by HESS After the standard quality selection procedure [80] and dead time correction, the data set amounts to ~400 hours of live time and a mean zenith angle of all observations is ~30° resulting in a typical energy threshold of 200 GeV.

Following the standard calibration of the shower images from photomultiplier tube signals [81], the event reconstruction scheme using the combined *Model-Hillas* analysis is applied to the data to select the gamma events. The *Hillas* reconstruction is based on the Hillas geometrical moment of the image [82]. The *model* analysis is based on a pixel-by-pixel comparison of the image to a template image generated by a semi-analytical model of the shower [83]. Both methods yield a typical energy resolution of 15% and an angular resolution at 68% full containment radius better than 0.1°. The data analysis is done with a combination of these two methods to improve the hadronic background rejection [82]. An additional cut on the primary interaction depth is also used to improve background rejection. After a cleaning of the images, the direction, energy, impact parameter, and primary interaction point are reconstructed for each gamma event. A cut on the image size at 60 photoelectrons is used to obtain better sensitivity to weak gamma-ray excesses. The background level is estimated using the template model method [84] as described below. This allows to estimate the background level at each sky position.

C. Gamma-ray sensitivity map

In order to study the HESS sensitivity in the galactic plane survey to dark matter annihilations from minispikes, we perform the analysis on the galactic plane survey data. The HESS flux sensitivity map is derived using the following sky maps in galactic coordinates, which are estimated within the survey range:

(i) the observed gamma-ray map,
(ii) the normalized measured background map,
(iii) the effective time exposure map (in seconds),
(iv) the gamma-ray acceptance map (in m^2).

The gamma-ray map is obtained after the event selection and reconstruction procedures described above. The sky map is divided into bins of $0.02° \times 0.02°$ size and an oversampling radius of 0.1° is applied to the data. The oversampling smooths the map with a top-hat function of radius of 0.1° to match the point spread function of the instrument. In each bin of the map in galactic coordinates, the background rate is estimated by the template background method (see [84] for details) and the normalized background map is obtained by the following relation:

$$N_{\mathrm{Bkg}}^{\mathrm{Norm}}(b, l) = N_{\mathrm{Bkg}}(b, l) \times \frac{\mathrm{Acc}_{\gamma}(b, l)}{\mathrm{Acc}_{\mathrm{h}}(b, l)}, \tag{7}$$

where the acceptances for gamma-ray-like events Acc_{γ} and hadronlike events $\mathrm{Acc}_{\mathrm{h}}$ are computed in each position of galactic longitude b and latitude l taking into account collection area corrections. Using the observed gamma-ray map and the normalized background map, we derive a sensitivity map expressed in terms of an upper limit (at 90% C.L) on the number of gamma events above the nominal energy threshold in each sky position. Using the exposure and acceptance maps, the flux sensitivity map for gamma-rays from dark matter annihilation is then determined by

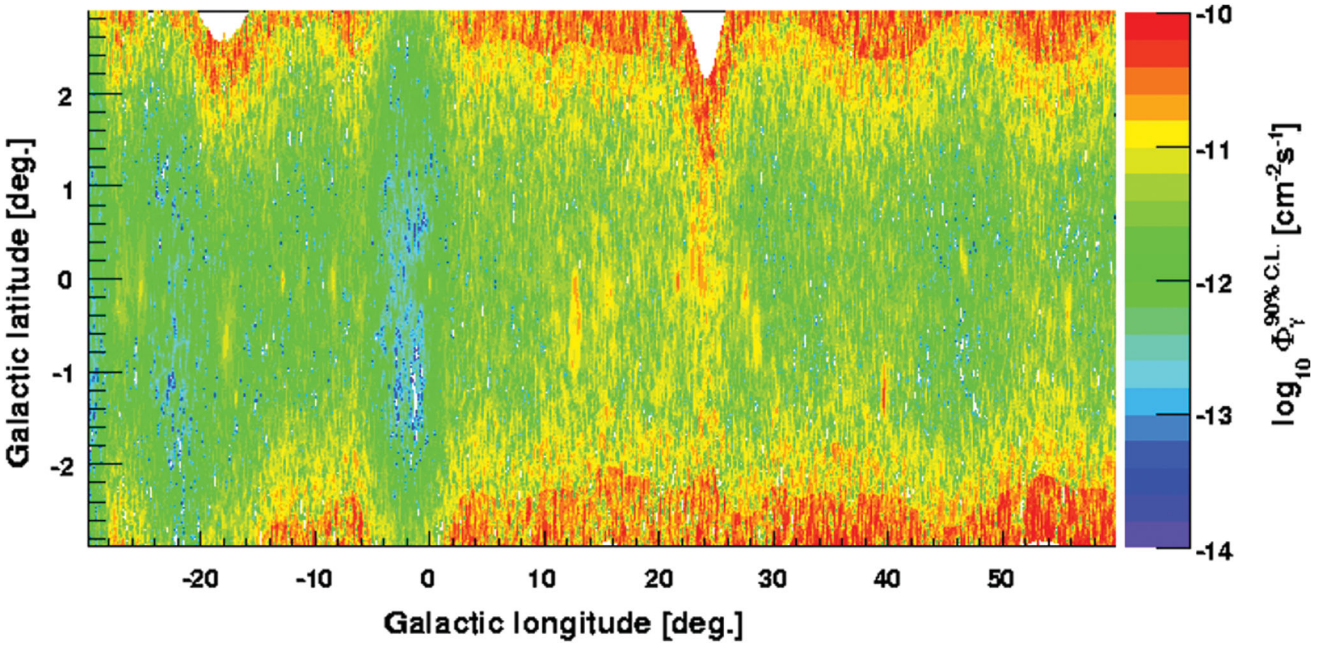

FIG. 4 (color). HESS sensitivity map in galactic coordinates, i.e. 90% C.L. limit on the integrated gamma-ray flux above 100 GeV, for dark matter annihilation assuming a dark matter particle of mass $m_{\chi} = 500$ GeV and annihilation into the $b\bar{b}$ channel. The flux sensitivity is correlated to the exposure and acceptance maps. In the galactic latitude band between $-2°$ and 2°, the gamma-ray flux sensitivity reaches 10^{-12} cm^{-2} s^{-1}.

$$\Phi_\gamma^{90\%\,\mathrm{C.L}}(b,l) = \frac{N_\gamma^{90\%\,\mathrm{C.L}}(b,l)\int_{E_{\mathrm{th}}}^{m_{\mathrm{DM}}}\frac{dN}{dE_\gamma}(E_\gamma)dE_\gamma}{\int_{T_{\mathrm{obs}}}\int_0^{m_{\mathrm{DM}}}A_{\mathrm{eff}}(E_\gamma, z(b,l), \theta(b,l))\frac{dN}{dE_\gamma}(E_\gamma)dE_\gamma d\tau}. \quad (8)$$

Here, A_{eff} is the effective area for gamma rays, which is a function of the gamma energy E_γ and the sky position (b, l). The $d\tau$ integration denotes the averaging according to the zenith angle z and offset θ distribution of the observation live time. The annihilation spectrum of the dark matter particle of mass m_{DM} is denoted by dN/dE_γ and is integrated from the nominal energy threshold E_{th}, which is about 100 GeV in the survey, up to m_{DM}. The integral over τ is calculated over the total observation live time T_{obs}.

Figure 4 shows the experimentally observed sensitivity map in the galactic plane from galactic longitudes $l = -30°$ to $l = +60°$ and galactic latitudes $b = -3°$ to $b = +3°$, for a dark matter particle of 500 GeV mass annihilating into the $b\bar{b}$ channel. The HESS sensitivity depends strongly on the exposure time and acceptance maps, which are related to the choice of the pointing positions. The flux sensitivity varies along the latitude and longitude due to inhomogeneous coverage of the galactic plane. In principle, the sensitivity map depends on the dark matter annihilation spectrum. However, as can be seen from Eq. (8), the spectrum is balanced by the effective area, which mainly drives the result of the integral. The particle mass is not expected to bring about strong variations in the map as long as the mass is larger than 100 GeV.

In the band between $-2°$ and $2°$ in galactic latitude, a DM annihilation flux sensitivity at the level of 10^{-12} cm^{-2} s^{-1} is achieved. HESS thus reaches the required sensitivity to be able to test dark matter annihilations from minispikes in the context of one relatively favorable scenario for IMBH formation and adiabatic growth of the DM halo around the black hole.

Deeper observations of the GC and at galactic longitude of $\sim -20°$ allow the flux sensitivity of $\sim 5 \times 10^{-13}$ cm^{-2} s^{-1} for a 500 GeV DM particle annihilating in the $b\bar{b}$ channel. For $b = 0°$ and $l = -6°$, the flux sensitivity is $\sim 10^{-12}$ cm^{-2} s^{-1}. For $|b| \geq 2°$, the sensitivity is deteriorated due to a weaker effective exposure. For $b = 0°$ and $l = -0.5°$, near the Galactic Center, the flux sensitivity is $\sim 10^{-13}$ cm^{-2} s^{-1} in the 100% BR $b\bar{b}$ annihilation channel and $\sim 5 \times 10^{-14}$ cm^{-2} s^{-1} in the $\tau^+\tau^-$ channel.

IV. RESULTS AND DISCUSSION

HESS observations (2004–2006) of the galactic plane allowed to discover more than 20 VHE sources [85]. Some of them have been identified owing to their counterparts at other wavelengths, but almost half of the sources have no obvious counterpart and are still unidentified [86]. For these sources, an accurate reconstruction of their energy spectra has been carried out. All spectra were consistent with a pure power law of spectral indices between 2.0 and 2.5, spanning up to 2 orders of magnitude in energy above the energy threshold, as shown in Fig. 8 of Ref. [86]. None of them exhibits an energy cutoff, characteristic of dark matter annihilation spectra, in the energy range from $\sim$100 GeV up to 10 TeV. Furthermore, the detailed study of their morphology [86] shows that all the sources have an intrinsic spatial extension greater than $\sim 5'$, while minispikes are expected to be pointlike sources, since the bulk of the gamma-ray emission comes from a region of size $\approx 10^{-3}$ pc at a typical distance from GC of 10 kpc. In the survey region discussed here, only three pointlike gamma-ray sources are detected: HESS J1826-148, HESS J1747-281, and HESS J1745-290. They are identified with well-known objects: LS 5039, G0.9 + 0.1 and the Galactic Center, respectively. HESS has detected so far no IMBH candidate within the survey range.

Based on the absence of plausible IMBH candidates in the HESS data, we can derive constraints on one scenario for neutralino or LKP dark matter annihilations. These constraints are shown as upper limits on the annihilation cross section (Figs. 6 and 7) but are actually constraints on

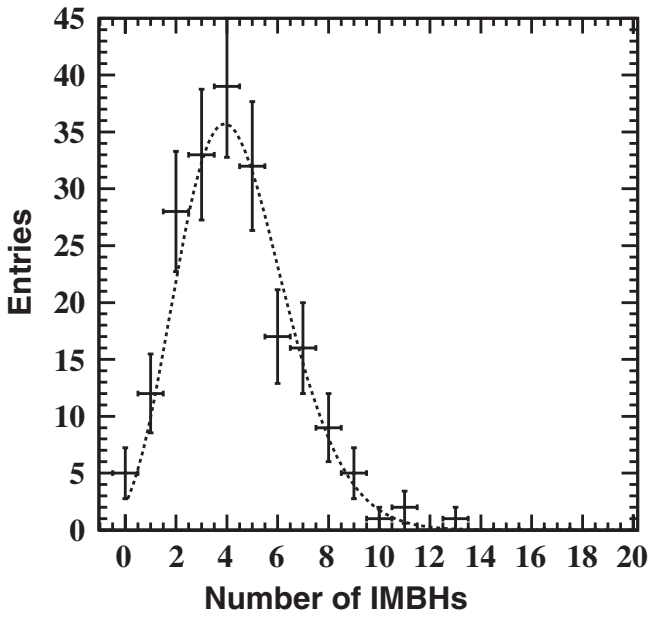

FIG. 5. Distribution of the number of IMBHs for the scenario B in the survey range corresponding to a field of view between $\pm 3°$ in galactic latitude and from $-30°$ to $60°$ in galactic longitude. The distribution is obtained from 200 stochastic realizations of Milky Way-like halos (see Sec. II A for details). The mean of the distribution is 4.3 with an r.m.s of 2.3. The distribution is well fitted to a Poisson distribution with mean 4.4 (black dashed line).

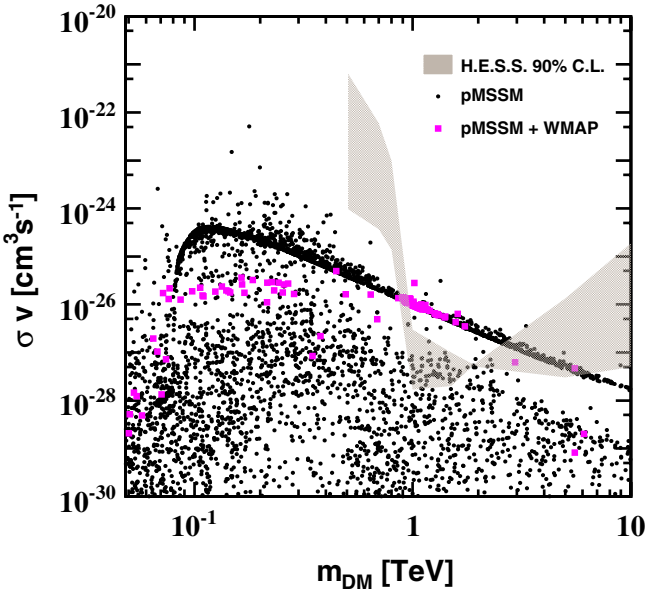

FIG. 6 (color online). Constraints on the IMBH gamma-ray production scenario for different neutralino parameters, shown as upper limits on the annihilation cross section σv as a function of the mass of the dark matter particle m_{DM}, but with a number of implicit assumptions about the IMBH initial mass function and halo profile (see text for details). For scenario B, the probability of having no observable halos in our galaxy is 10% from Poisson statistics making these limits essentially 90% confidence level exclusion limits for this one particular (albeit optimistic) scenario.

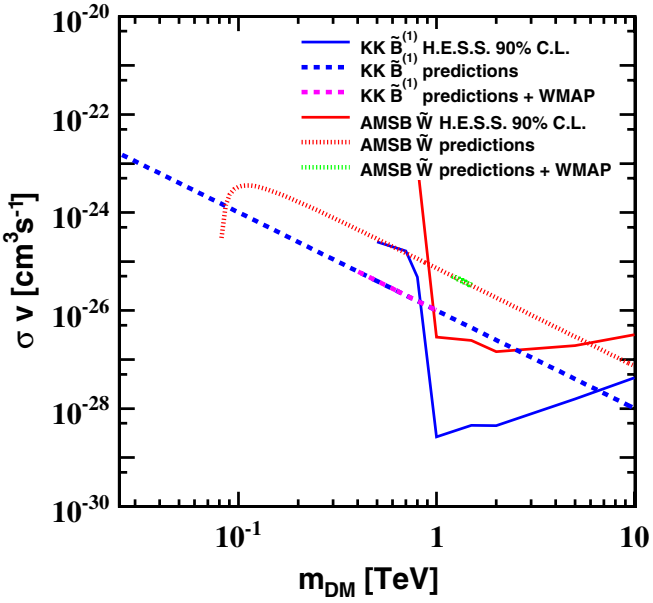

FIG. 7 (color online). 90% C.L. exclusion limits on the annihilation cross section σv as a function of the mass of the dark matter particle m_{DM} for a Kaluza-Klein boson $\tilde{B}^{(1)}$ (solid blue line) and a pure wino $\tilde{W}$ in AMSB (solid red line). The limit is derived from the HESS flux sensitivity in the galactic plane survey within the minispike scenario. Kaluza-Klein models in UED scenario (blue dashed line) and AMSB models (red dotted line) are plotted together with those satisfying the WMAP constraints on the dark matter particle relic density (pink dashed line and green dotted line, respectively).

the entire gamma-ray production scenario, assuming the mass function of scenario B and a coreless halo model. In the survey range, the expected mean number of IMBHs is 4.3, within the assumptions of scenario B, as shown in Fig. 5. The number of IMBHs in the whole halo depends on the assumed cosmological parameters in the formation scenario [87], in particular, the reionization redshift. The value of 4.3 *unmerged* IMBHs is for a reionization redshift of 16. The redshift of 10.8 ± 1.4 determined from latest Wilkinson Microwave Anisotropy Probe (WMAP) data [88] favors a larger number of IMBHs, since they had less time for merger events to occur [87]. The distribution of the IMBH number has an intrinsic r.m.s of 2.3. The probability to find no IMBH in the survey range is 2.5%. The simulations of the Milky Way halo show that the IMBH number distribution in the sky survey range is well fitted with a Poisson distribution with mean 4.4.

For a given gamma-ray flux sensitivity Φ, we define the probability density function of black holes yielding an integrated gamma-ray flux larger than Φ, $d^2N_{\mathrm{BH}}(>\Phi)/dbdl$, from the IMBH catalog used in [38] by

$$N_{\mathrm{BH}}(\mathrm{detected}, >\Phi) = \int_{b=-3^\circ}^{b=+3^\circ} \int_{l=-30^\circ}^{l=+60^\circ} \frac{d^2N_{\mathrm{BH}}(>\Phi)}{dbdl} dbdl. \quad (9)$$

$N_{\mathrm{BH}}(\mathrm{detected}, >\Phi)$ denotes the expected number of black holes yielding a gamma-ray flux larger than Φ in the survey, Φ corresponding to the HESS sensitivity. The total number of black holes in the survey is computed by integrating the probability density function $d^2N_{\mathrm{BH}}(>\Phi)/dbdl$ over the latitude and longitude ranges of the galactic plane survey. Since no HESS source is a plausible IMBH candidate, we thus calculate for each dark matter particle mass the limit at 90% C.L. on the velocity-weighted cross section σv, assuming a Poisson distribution.

Figure 6 shows the exclusion limit at the 90% C.L. on σv as a function of the neutralino mass m_{DM}. The neutralino is assumed to annihilate into $b\bar{b}$ and $\tau^+\tau^-$ with 100% BR, respectively. Below ~2 TeV, the upper contour of the gray shaded area is given by the $b\bar{b}$ assumption and yields the conservative exclusion limit. Above 2 TeV, the upper contour corresponds to the $\tau^+\tau^-$ annihilation spectrum. The maximum sensitivity of HESS to DM annihilation for the $b\bar{b}$ channel is achieved for masses of order 5 TeV as expected from Fig. 3. For neutralino masses in the TeV energy range, we obtain limits on one minispike scenario (scenario B) The limits on σv are at the level of 10^{-28} cm^{-3} s^{-1} for the $b\bar{b}$ channel. A rapid decrease in sensitivity is observed for WIMP masses less than

TABLE I. pMSSM parameter space randomly scanned to generate SUSY models. A set of parameters corresponds to a specific pMSSM model.

Parameter	Minimum	Maximum
m_0	1 TeV	30 TeV
M_2	1 TeV	50 TeV
μ	1 TeV	50 TeV
m_A	1 TeV	50 TeV
$A_{t,b}$	−300 GeV	+300 GeV
$\tan\beta$	3	60

~800 GeV. This corresponds to the threshold effect seen in Fig. 3. Predictions for SUSY models are generated using the DarkSUSY code [89] in a phenomenological MSSM (pMSSM) framework characterized by the following independent parameters: the common scalar mass m_0, the gaugino mass parameter M_2, the higgsino mass parameter μ, the *CP*-odd Higgs mass M_A, the trilinear couplings $A_{t,b}$, and the Higgs vacuum expectation value ratio $\tan\beta$. The set of parameters for a given model is randomly chosen in the pMSSM parameter space encompassing a large class of pMSSM models, as described in Table I. Models providing a neutralino thermal relic density $\Omega_{\rm DM}h^2$ in the range $[0.08, 0.12]$ are overlaid to account for the cold dark matter density inferred from the measurements of the cosmic microwave background anisotropies of the WMAP satellite. Some models in the mass range 0.8–6 TeV can be excluded.

Figure 7 shows the 90% C.L. exclusion limit on σv as a function of the DM particle mass $m_{\rm DM}$ in the case of AMSB and Kaluza-Klein scenarios. In both cases, the BRs of each annihilation channel entering in the calculation of the total annihilation differential spectra are uniquely determined as discussed in Sec. II. In the AMSB scenario, the neutralino is considered here to be a pure wino annihilating with 100% BR into the W^+W^- channel. The predictions for σv are parameterized using the results of [90], where it is derived in the case of the latter assumption on the annihilation scheme. The AMSB models fulfilling in addition the WMAP constraints are overlaid. Models yielding neutralino masses between 900 GeV and 6 TeV are excluded including those having a neutralino thermal relic density compatible with the WMAP measurements. Predictions on the annihilation cross section for pairs of $\tilde{B}^{(1)}$ from UED theories [91] are also plotted as well as those satisfying the WMAP constraints. In this scenario, $\tilde{B}^{(1)}$ masses in the range from 0.8 to 6 TeV can be excluded.

V. SUMMARY

Observational clues for the existence of IMBHs start to accumulate. If they indeed exist, IMBH could be dark matter annihilation boosters. The prospects for detecting dark matter annihilation around IMBHs have been widely discussed in the literature [36,38,39,92–94]. In this work, we derive the first experimental constraints on the minispike scenario of Ref. [38].

Using HESS data collected in the galactic plane survey, we show that HESS has the required sensitivity to probe gamma rays from dark matter annihilation in minispikes around IMBHs believed to populate the Milky Way halo. The new analysis using ~400 hours of data taken in the galactic plane but not foreseen initially for this purpose, allows to derive flux sensitivity limits for indirect dark matter search. Combining all the survey data, the gamma-ray flux sensitivity map is derived for dark matter annihilation in the region $[-30°, 60°]$ in longitude and $[-3°, 3°]$ in latitude. We show that HESS reaches a flux sensitivity of $\sim 10^{-12}$ cm^{-2} s^{-1} above 100 GeV.

For the first time, a clumpiness scenario has been tested in a large field of view with an imaging atmospheric Cherenkov telescope. Strong constraints are obtained in one of the two IMBH formation scenarios discussed [38] (scenario B). The absence of plausible candidates for galactic IMBHs in the HESS Galactic plane data set allows us to put constraints on one of the more optimistic scenarios for detecting neutralino or LKP annihilation from minispikes around IMBHs. The first experimental exclusion limits at 90% C.L. on the velocity-weighted annihilation cross section as a function of the dark matter particle mass within the minispike scenario are derived. Predictions from various WIMP particle physics scenarios are constrained.

Since the characteristic annihilation flux from a IMBH varies as $(\sigma v)^{2/7}$, reflecting the depletion of the inner part of dark matter halo due to annihilation during the lifetime of the IMBH, limits derived on σv in the absence of a detection are proportional to $(\Phi_{\rm min}/\Phi_{\rm ref})^{7/2}$, where $\Phi_{\rm min}$ is the sensitivity limit and $\Phi_{\rm ref}$ the predicted annihilation flux for a nominal value of σv. Uncertainties in $\Phi_{\rm ref}$, reflecting, for example, the imperfect knowledge of the exact shape of the dark matter spike close to the IMBH, cause correspondingly enlarged uncertainties on the limits on σv. Similarly, variations in the predicted number and mass of IMBHs may influence the limits; for example, at least about 50 IMBHs have to be contained in the galactic halo in order to set a meaning flux upper limit, given the limited solid angle coverage of the HESS survey. The limits given here apply within the formalism and approximations of scenario B of [38].

The analysis described here can be adapted to other particle physics parameters, e.g. different types of DM particles and annihilation channels. Constraints are derived within the minispike scenario although the method developed here is generic and is suited to whatever the assumed dark matter clump scheme. The flux sensitivity map is a powerful tool to investigate the sensitivity to other types of

overdensities such as small scale clumps [17,18,95,96] or compact dark matter structures like spikes [25,76,97–99].

ACKNOWLEDGMENTS

The support of the Namibian authorities and of the University of Namibia in facilitating the construction and operation of HESS is gratefully acknowledged, as is the support by the German Ministry for Education and Research (BMBF), the Max Planck Society, the French Ministry for Research, the CNRS-IN2P3 and the Astroparticle Interdisciplinary Programme of the CNRS, the U.K. Particle Physics and Astronomy Research Council (PPARC), the IPNP of the Charles University, the South African Department of Science and Technology and National Research Foundation, and by the University of Namibia. We appreciate the excellent work of the technical support staff in Berlin, Durham, Hamburg, Heildelberg, Palaiseau, Paris, Saclay, and in Namibia in the construction and operation of the equipment. We thank Andrew Zentner for making the IMBH catalog available for this work.

[1] D. N. Spergel, R. Bean, O. Doré *et al.*, Astrophys. J. Suppl. Ser. **170**, 377 (2007).
[2] L. Bergström, Rep. Prog. Phys. **63**, 793 (2000).
[3] G. Bertone, D. Hopper, and J. Silk, Phys. Rep. **405**, 279 (2005).
[4] G. Jungman, M. Kamionkowski, and K. Griest, Phys. Rep. **267**, 195 (1996).
[5] T. Appelquist, H.-C. Cheng, and B. A. Dobrescu, Phys. Rev. D **64**, 035002 (2001).
[6] H. Cheng, J. Feng, and K. Matchev, Phys. Rev. Lett. **89**, 211301 (2002).
[7] G. Servant and T. Tait, Nucl. Phys. **B650**, 391 (2003).
[8] J. Silk and H. Bloemen, Astrophys. J. Lett. **313**, L47 (1987).
[9] E. A. Baltz, C. Briot, P. Salati *et al.*, Phys. Rev. D **61**, 023514 (1999).
[10] N. Fornengo, L. Pieri, and N. Scopel, Phys. Rev. D **70**, 103529 (2004).
[11] C. Calcaneo and B. Moore, Phys. Rev. D **62**, 123005 (2000).
[12] A. Tasitsiomi and A. V. Olinto, Phys. Rev. D **66**, 083006 (2002).
[13] F. Stoehr *et al.*, Mon. Not. R. Astron. Soc. **345**, 1313 (2003).
[14] S. M. Koushiappas, A. R. Zentner, and T. P. Walker, Phys. Rev. D **69**, 043501 (2004).
[15] E. A. Baltz, J. E. Taylor, and L. L. Wai, ApJL (unpublished).
[16] L. Pieri, E. Branchini, and S. Hofmann, Phys. Rev. Lett. **95**, 211301 (2005).
[17] S. M. Koushiappas, Phys. Rev. Lett. **97**, 191301 (2006).
[18] J. Diemand, M. Kuhlen, and P. Madau, Astrophys. J. **657**, 262 (2007).
[19] L. Pieri, G. Bertone, and E. Branchini, Mon. Not. R. Astron. Soc. **384**, 1627 (2008).
[20] F. A. Aharonian *et al.* (HESS Collaboration), Phys. Rev. Lett. **97**, 221102 (2006).
[21] G. Zaharijas and D. Hooper, Phys. Rev. D **73**, 103501 (2006).
[22] S. Profumo, Phys. Rev. D **72**, 103521 (2005).
[23] Y. Mambrini, C. Munoz, E. Nezri, and F. Prada, J. Cosmol. Astropart. Phys. 01 (2006) 010.
[24] A. Cesarini, F. Fucito, A. Lionetto, A. Morselli, and P. Ullio, Astropart. Phys. **21**, 267 (2004).
[25] G. Bertone and D. Merritt, Phys. Rev. D **72**, 103502 (2005).
[26] M. Mateo, Annu. Rev. Astron. Astrophys. **36**, 435 (1998).
[27] N. Evans, F. Ferrer, and S. Sarkar, Phys. Rev. D **69**, 123501 (2004).
[28] S. Profumo and M. Kamionkowski, J. Cosmol. Astropart. Phys. 03 (2006) 003.
[29] M. Sanchez *et al.*, Phys. Rev. D **76**, 123509 (2007).
[30] L. Bergström and D. Hooper, Phys. Rev. D **73**, 063510 (2006).
[31] L. Strigari *et al.*, Phys. Rev. D **75**, 083526 (2007).
[32] F. A. Aharonian *et al.* (HESS Collaboration), Astropart. Phys. **29**, 55 (2008).
[33] B. Willman *et al.*, Astrophys. J. **626**, L85 (2005).
[34] M. Irwin *et al.*, Astrophys. J. **656**, L13 (2007).
[35] S. Walsh, H. Jerjen, and B. Willman, ApJL (unpublished).
[36] H. S. Zhao and J. Silk, Phys. Rev. Lett. **95**, 011301 (2005).
[37] G. Bertone and D. Merritt, Mod. Phys. Lett. A **20**, 1021 (2005).
[38] G. Bertone, A. Zentner, and J. Silk, Phys. Rev. D **72**, 103517 (2005).
[39] G. Bertone, Phys. Rev. D **73**, 103519 (2006).
[40] http://www-glast.stanford.edu/.
[41] PYTHIA package.
[42] A. H. Chamseddine, A. Arnowitt, and P. Nath, Phys. Rev. Lett. **49**, 970 (1982).
[43] L. J. Hall, J. Kykken, and S. Weinberg, Phys. Rev. D **27**, 2359 (1983).
[44] N. Otha, Prog. Theor. Phys. **70**, 542 (1983).
[45] R. Barbieri, S. Ferrara, and C. Savoy, Phys. Lett. B **119**, 343 (1982).
[46] L. Randall and R. Sundrum, Nucl. Phys. **B557**, 79 (1999).
[47] G. Guidice *et al.*, J. High Energy Phys. 12 (1998) 027.
[48] D. Hooper and L. Wang, Phys. Rev. D **69**, 035001 (2004).
[49] C. L. Fryer and V. Kalogera, Astrophys. J. **554**, 548 (2001).
[50] J. M. Silverman and A. V. Filippenko, arXiv:0802.2716 [Astrophys. J. (unpublished)].
[51] L. Ferrarese and H. Ford, Space Sci. Rev. **116**, 523 (2005).
[52] J. E. Greene and L. C. Ho, Astrophys. J. **670**, 92 (2007).
[53] E. Colbert and A. Ptak, Astrophys. J. Suppl. Ser. **143**, 25 (2002).
[54] D. A. Swartz, K. K. Ghosh, A. F. Tennant, and K. W. Wu, arXiv:astro-ph/0405498.

[55] G. C. Dewangan, R. E. Griffiths, M. Choudhury, T. Miyaji, and N. J. Schurch, Astrophys. J. **635**, 198 (2005).
[56] J. Frank and M. J. Rees, Mon. Not. R. Astron. Soc. **176**, 633 (1976).
[57] E. Noyola, K. Gebhardt, and M. Bergmann, Astrophys. J. **676**, 1008 (2008).
[58] B. M. Peterson *et al.*, Astrophys. J. **632**, 799 (2005).
[59] Z. Haiman and A. Loeb, Astrophys. J. **552**, 459 (2001).
[60] R. Islam, J. Taylor, and J. Silk, Mon. Not. R. Astron. Soc. **340**, 647 (2003).
[61] M. Volonteri, F. Haardt, and P. Madau, Astrophys. J. **582**, 559 (2003).
[62] S. M. Koushiappas, J. S. Bullock, and A. Dekel, Mon. Not. R. Astron. Soc. **354**, 292 (2004).
[63] P. Madau and M. J. Rees, Astrophys. J. Lett. **551**, L27 (2001).
[64] A. Heger, C. L. Fryer, S. E. Woosley, N. Langer, and D. H. Hartmann, Astrophys. J. **591**, 288 (2003).
[65] M. G. Haehnelt and M. J. Rees, Mon. Not. R. Astron. Soc. **263**, 168 (1993).
[66] A. Loeb and F. A. Rasio, Astrophys. J. **432**, 52 (1994).
[67] D. J. Eisenstein and A. Loeb, Astrophys. J. **443**, 11 (1995).
[68] M. G. Haehnelt, P. Natarajan, and M. J. Rees, Mon. Not. R. Astron. Soc. **300**, 817 (1998).
[69] O. Y. Gnedin, Classical Quantum Gravity **18**, 3983 (2001).
[70] V. Bromm and A. Loeb, Astrophys. J. **596**, 34 (2003).
[71] D. N. C. Lin and J. E. Pringle, Mon. Not. R. Astron. Soc. **225**, 607 (1987).
[72] S. L. Shapiro and S. A. Teukolsky, *Black Holes, White Dwarfs, and Neutron Stars* (Wiley-Interscience, New York, 1983).
[73] Since merger events are likely to perturb the DM distribution around a IMBH, only those IMBH will be considered which never experienced a major merger.
[74] G. D. Quinlan, L. Hernquist, and S. Sigurdsson, Astrophys. J. **440**, 554 (1995).
[75] D. Merritt, arXiv:astro-ph/0301257.
[76] P. Gondolo and J. Silk, Phys. Rev. Lett. **83**, 1719 (1999).
[77] K. Bernlöhr *et al.*, Astropart. Phys. **20**, 111 (2003).
[78] P. Vincent *et al.*, *Proc. of the 28th International Cosmic Ray Conference*, edited by T. Kajita *et al.* (Universal Academy Press, Tokyo, 2003), p. 2887.
[79] S. Funk *et al.*, Astropart. Phys. **22**, 285 (2004).
[80] F. A. Aharonian *et al.* (HESS Collaboration), Astron. Astrophys. **457**, 899 (2006).
[81] F. A. Aharonian *et al.* (H.E.S.S. Collaboration), Astropart. Phys. **22**, 109 (2004).
[82] F. A. Aharonian *et al.* (HESS Collaboration), Astron. Astrophys. **430**, 865 (2005).
[83] M. de Naurois *et al.*, *Proc. Conf. Towards a Network of Atmospheric Cherenkov Detectors* (Palaiseau, France, 2005), p. 149.
[84] G. P. Rowell, Astron. Astrophys. **410**, 389 (2003).
[85] F. Aharonian *et al.* (HESS Collaboration), Astrophys. J. **636**, 777 (2006).
[86] F. Aharonian *et al.* (HESS Collaboration), Astron. Astrophys. **477**, 353 (2008).
[87] S. M. Koushiappas and A. R. Zentner, Astrophys. J. **639**, 7 (2006).
[88] E. Komatsu *et al.* (WMAP Collaboration), arXiv:0803.0547.
[89] P. Gondolo *et al.*, J. Cosmol. Astropart. Phys. 07 (2004) 008.
[90] T. Moroi and L. Randall, Nucl. Phys. **B570**, 455 (2000).
[91] E. Baltz and D. Hooper, J. Cosmol. Astropart. Phys. 07 (2005) 001.
[92] P. Brun, G. Bertone, J. Lavalle, P. Salati, and R. Taillet, Phys. Rev. D **76**, 083506 (2007).
[93] M. Fornasa, M. Taoso, and G. Bertone, Phys. Rev. D **76**, 043517 (2007).
[94] S. Horiuchi and S. Ando, Phys. Rev. D **74**, 103504 (2006).
[95] L. Pieri and E. Branchini, Phys. Rev. D **69**, 043512 (2004).
[96] L. Bergström, J. Edsjö, and P. Ullio, Phys. Rev. D **58**, 083507 (1998).
[97] G. Bertone and D. Merritt, Mod. Phys. Lett. A **20**, 1021 (2005).
[98] P. Ullio, H. Zhao, and M. Kamionkowski, Phys. Rev. D **64**, 043504 (2001).
[99] G. Bertone, G. Sigl, and J. Silk, Mon. Not. R. Astron. Soc. **337**, 98 (2002).